Chapter-VI

Synthesis of ternary CaNiAl-layered double hydroxide as a potential adsorbent and its effective removal of congo red and methyl orange dye from aqueous solution

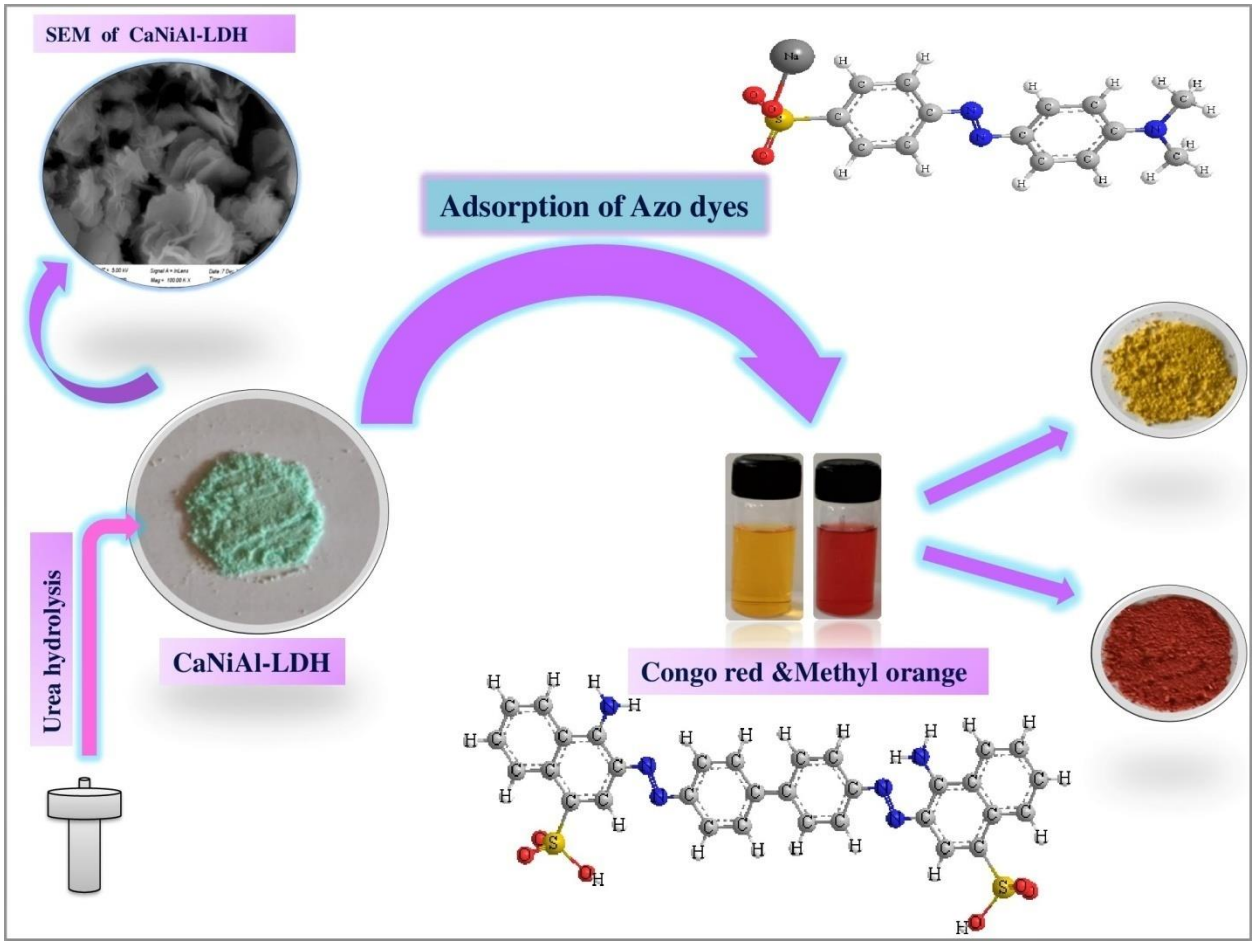

Chapter- VI

Synthesis of ternary CaNiAl-layered double hydroxide as a potential adsorbent and its effective removal of congo red and methyl orange dye from aqueous solution

VI.1 Introduction

With the fast growth of urbanisation, the discharge of effluents from various manufacturing industries has created an environmental hazard for all living species due to its diverse effects. Among several water pollutants, the use of synthetic azo dyes has emerged rapidly due to their wide applications in industries such as textile, plastic, leather, foods, cosmetics, medicine, and paper.[1] Dyes disperse in water bodies, leading to coloured water, which can block the radiation from sunlight and affect aquatic life forms. In addition, azo dyes have a complex and stable chemical structure that makes it very difficult to separate or degrade from water bodies via conventional methods. It is also highly toxic due to its known carcinogenic and mutagenic properties, and it also leads to variations in parameters such as BOD and COD levels that can prove to be detrimental for all living habitats. In particular, congo red (CR) and methyl orange (MO) dye, a type of azo dye, is highlighted very toxic and cause adverse effects such as cancer, irritation, photosynthesis inhibition, reduction in O_2 level, and suffocating flora and fauna.[2,3] Therefore, treatment of azo-dye polluted waste water to lower the levels of contaminants in industrial effluents is highly urgent.

In order to alleviate the negative impacts of toxic dyes, several methodologies and techniques were established for waste water treatment. Some widely used efficient techniques that can achieve dye separation from an aqueous medium are coagulation/flocculation,[4] filtration,[5] ozonation,[6] photodegradation,[7] and adsorption.[8] However, the adsorption method is deemed as one of the most preferred approaches in remediation of various toxins from the liquid phase. Due to its ease of operation, low cost, high efficiency, safe and mild reaction condition, it can be easily afforded in all developing nations. This technique can be applied to separate, purify, detoxify, and deodorize the toxic product in both liquid and gaseous mediums. A large number of adsorbents were reported for the removal of CR dye, for instance, MOF,[9] activated carbon,[10] polymer composite,[11] zeolite,[12] and LDH.[13] Moreover, LDH can be considered as one of the most suitable candidates for water pollutant treatment because of its numerous advantages

such as flexible structure, high surface area, thermal stability, ease of regeneration, and non-toxicity.

LDHs are broad class of anionic clays, which is generally represented by the chemical formula $[M_{1-x}^{2+}M_x^{3+}(OH_2)]^{x+}(A^{n-})_{x/n}.H_2O]$, where M^{2+}(Ca^{2+}, Mg^{2+}, Fe^{2+}, Ni^{2+} etc.), M^{3+}(Fe^{3+}, Al^{3+}, Cr^{3+}, etc.) and A^{n-}(CO_3^{2-}, Cl^-, NO_3^-, etc.) were divalent metal cations, trivalent metal cations, and interlayer ions, respectively. The basic architecture of LDH contains positively charged brucite layers intercalating various compensating anions. Designing LDH can be achieved through various synthetic routes such as hydrothermal, urea hydrolysis, co-precipitation, rehydration/construction, and ion exchange. In addition, anion exchange in the structure can be tuned by intercalating with various organic and inorganic ions, which plays a key role in the adsorption process.[14,15] Since the adsorption behaviour of binary metals containing LDH is highly explored, only a few reports on the utilization of ternary LDH as a dye treatment alternative are available. Consequently, to improve the sorption characteristics of binary LDH, the variation in the structure can be made by introducing third metal ions.

In this chapter, we attempt to synthesize ternary CaNiAl-LDH via urea hydrolysis method. The as-synthesized sorbents were implemented for the removal of targeted azo-dye CR and MO from aqueous solutions. The influence of the adsorption parameters such as pH, temperature, dosages, contact time, and initial dye concentration on the adsorption performances was investigated. The reusability studies are also conducted. The isotherm and kinetic studies were also reported, and the plausible mechanism of dye sorption were also analysed by recording PXRD and FT-IR spectra of the sample after adsorption of targeted pollutants.

VI. 2 Materials and Methods

Nickel chloride hexahydrate ($NiCl_2.6H_2O$), Calcium chloride dihydrate ($CaCl_2.2H_2O$), Aluminium chloride ($AlCl_3$), Sodium Hydroxide (NaOH) were procured from Merck. Urea (NH_2CONH_2), Congo red ($C_{32}H_{22}N_6Na_2O_6S_2$) and Methyl orange ($C_{14}H_{14}N_3NaO_3S$) was purchased from Qualigens India Pvt. Ltd. All the obtained chemicals are of analytical grade and utilized directly without any further purifications.

VI.2.1 Preparation of adsorbents

The sample was prepared via a facile urea hydrolysis method. Initially, a mixture of metal precursor's solutions containing 8 mmol $NiCl_2.6H_2O$, 8 mmol $CaCl_2.H_2O$, and 4 mmol $AlCl_3$ in a 100 mL aqueous solution was stirred in a beaker. Subsequently, 2.1 g of urea was further added to the solution mixture and continuously stirred until the precursors were completely dissolved. The resulting suspension is then transferred into an autoclave and heated at 150 ℃ in an oven for 6 hours. The obtained green precipitate was collected and washed several times with deionised water. Finally, the resulting product was dried in a vacuum at 50 ℃ and crushed with mortar to obtain the powder form denoted as CaNiAl-LDH.

VI.2.2 Adsorption Experiment

To investigate the adsorption efficiency of ternary CaNiAl-LDH, the adsorption isotherm experiment was conducted in batch mode. In isotherm studies, a stock solution of CR dye having an initial concentration of 30 to 270 mg/L and methyl orange (10-110 mg/L) was prepared in distilled water. 20 mL of dye solution at varying initial concentration was taken in a conical flask, and 0.025 g of the adsorbent was mixed. The resulting solution was then allowed to stir at room temperature (28 ℃) in a water bath shaker for time period of 6 hours to attain equilibrium. The adsorbent was separated from the liquid suspension by filtration, and the concentration of CR and MO dye in the filtrate was measured by using a UV-Spectrophotometer at absorption wavelengths of 498 and 464 nm. The percentage removal and quantity of CR adsorbed on to CaNiAl-LDH were calculated by the given equation:

$$\% \text{ of dye removal} = \frac{(C_0 - C_e) \times 100}{C_0} \tag{6.1}$$

$$q_e = \frac{(C_0 - C_e)\, V}{W} \tag{6.2}$$

where, C_0 and C_e denotes initial and equilibrium dye concentration, respectively. q_e indicates the amount of dye adsorbed at equilibrium, V represents the volume of the adsorbate solution (mL), and W signifies the quantity of adsorbent (g).

In kinetic studies, 0.025 g of the adsorbent CaNiAl-LDH was mixed with 20 mL of dye solution at the initial dye concentration (50 mg/L). The liquid suspension is then allowed to agitate in a shaker for a time period of 260 min. After a definite time interval, 2 mL of the solution was withdrawn and separated from the adsorbent by centrifugation at 1000 rpm/min. Similarly, the residual dye concentration was estimated at a maximum absorption wavelength of 498 and 464 nm for CR and MO dye, respectively. The quantity of dye uptake at time *t* was evaluated by the equation:

$$q_t = \frac{(C_0 - C_t)\,V}{W} \qquad (6.3)$$

where, q_t represents the amount of dye adsorbed at time *t*, and C_t indicates the concentration of dye at time *t*.

VI. 3 Results and Discussion

VI. 3.1 Powder X-ray Diffraction study

The PXRD spectrum of synthesized CaNiAl-LDH before and after sorption of CR and MO dye is depicted in **Fig VI.1**. The characteristic pattern of the typical layered double hydroxide structure was exhibited in pristine CaNiAl-LDH. The peaks observed at 2θ values (11.34, 22.94, 34.88, 39.17, 46.48, 60.75, 62.17) were attributed to the corresponding indexed plane (003, 006, 009, 015, 018, 110, 113), respectively.[16] The sharp reflection manifested in the XRD spectrum further corroborates with the well-crystalline nature of the as-synthesized sample. The cell parameters a denotes the metal-metal distance in the LDH sheets, while the parameter c represents the interlayer distance in brucite sheets, which is three times the values of basal spacing. However, the evaluated values of a = 0.3 nm and c = 2.34 nm based on expressions ($a = 2d_{110}$, $c = 3d_{003}$) were found almost constant for CaNiAl-LDH, CaNiAl-LDH-CR, and CaNiAl-LDH-MO. Since the shifting of peaks was not observed after adsorption of CR and MO dye, it can be anticipated that sorption takes place on the external surface rather than intercalation on the interlamellar spaces.[17]

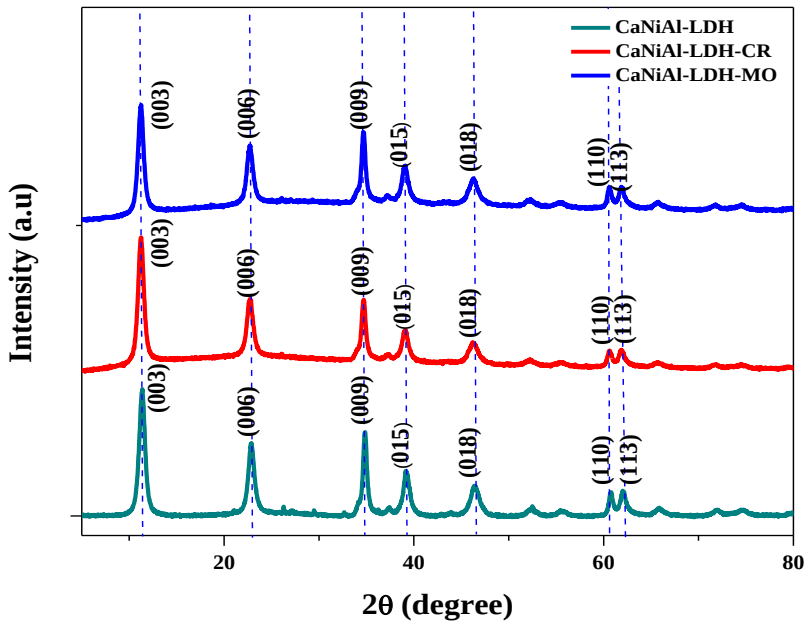

Fig VI.1: PXRD pattern of CaNiAl-LDH before and after adsorption of CR and MO dye.

VI. 3.2 FT-IR analysis

The identification of surface functionalities was performed by FTIR analysis, as shown in **Fig. VI.2.** The broad band at 3489 cm^{-1} arises due to the –OH stretching vibration of the water molecule. Another band detected at 1641 cm^{-1} is attributed to the bending vibration of the –OH group. The sharp absorption peak at 1370 cm^{-1} is assigned to the interlayer NO_3^- ion, and the low intensity band between 600 and 800 cm^{-1} was noticed due to M-O stretching vibration (Ca-O, Al-O, Ni-O). After adsorption of the CR molecule, the spectrum of CaNiAl-LDH-CR manifested two small new peaks at 1043 cm^{-1} and 522 cm^{-1}, which confirms that sorption of CR over the surface of the adsorbent occurred. In addition, the intensity of the peaks also decreased after adsorption in comparison to pristine CaNiAl-LDH. The peak at 1588 cm^{-1} in CaNiAl-LDH-MO is due to -N=N- stretching vibration. Thus, the result was consistent and strongly suggests the active role of surface functional groups during the adsorption of targeted pollutants.[18, 19]

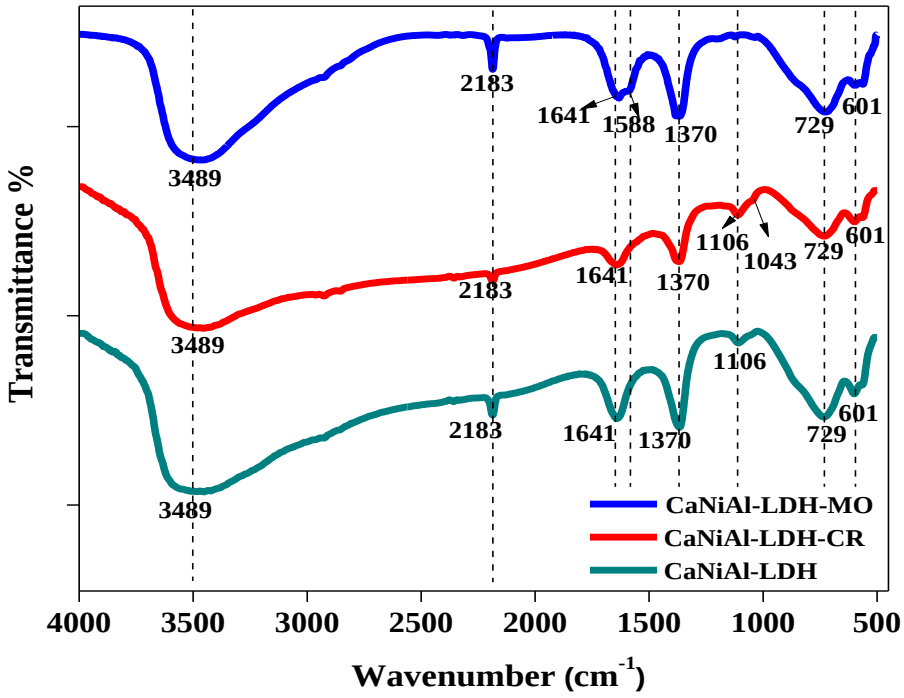

Fig VI.2: FT-IR spectra of CaNiAl-LDH before and after adsorption of CR and MO dye.

VI. 3.3 BET surface area analysis

Fig VI.3 illustrates the N_2-adsorption desorption isotherms of ternary CaNiAl-LDH; the insets of **Fig VI.3** showed the pore size distribution curve determined based on BJH method of the sample. The isotherm curve is consistent with type-IV isotherm and H3-hysteresis loop, which signifies the presence of mesopores on the material. In **Fig VI.3**, it is seen that the isotherm curve generates slowly at a higher relative pressure ($P/P_0 < 0.8$), which depicts the inter particle mesoporosity of CaNiAl-LDH. The specific surface area, pore size, and pore volume of the as-synthesized sample were 58.45 m/g, 3.85 nm, and 0.106 cc/g, respectively.[20]

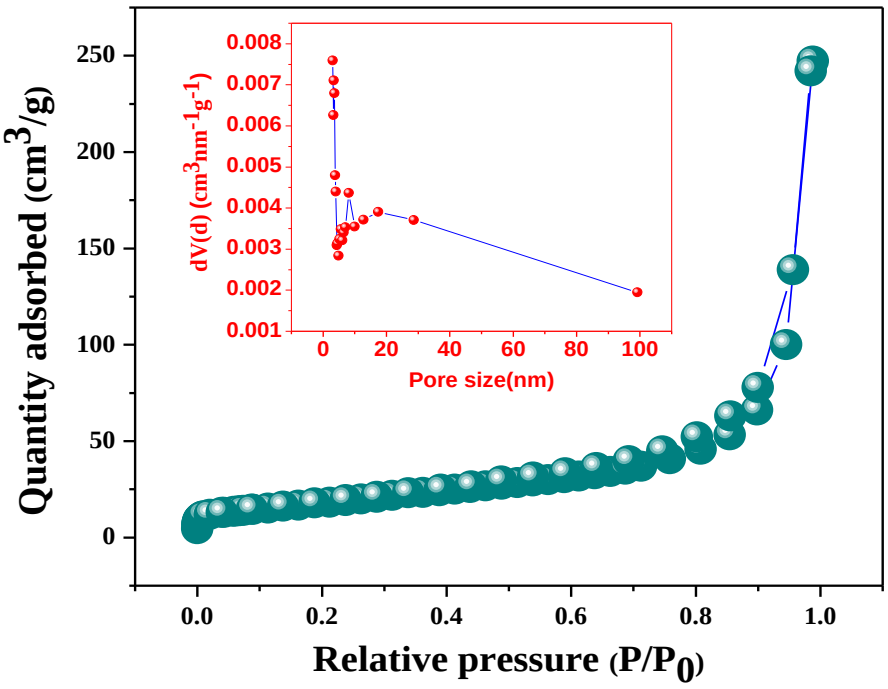

Fig VI.3: N_2-adsorption desorption isotherm curve of CaNiAl-LDH.

VI. 3.4 Thermogravimetric Analysis

The mass decomposition of the synthesized sample CaNiAl-LDH was studied by thermogravimetric analysis and is depicted in **Fig VI.4**. The TGA curve shows that mass losses take place at three different stages. The initial mass loss of 11.62 % in the region between (30 ℃ -220 ℃) was observed due to the elimination of physio adsorbed water molecules. The highest mass loss of 19.07 % takes place in the second step around (220-574 ℃), which can be ascribed to the removal of interlayer ions such as NO_3^-, CO_3^{2-}, and Cl^-. Moreover, the final stage of mass loss (4.4 %) arises between 574 and 721 ℃, where the layered structure of CaNiAl-LDH gets completely destructed and beyond 720 ℃ the curve appears to be a constant straight line without further mass loss.[21]

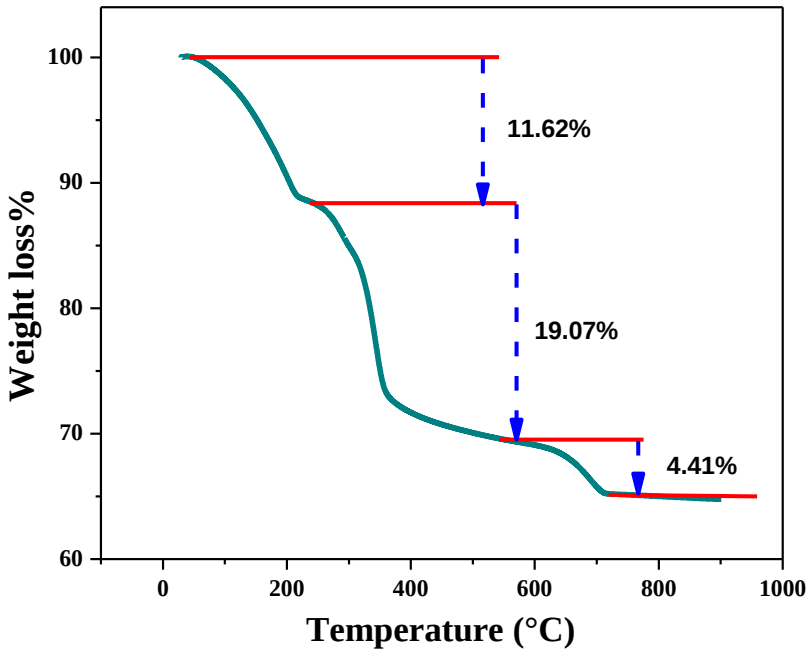

Fig VI.4: TGA profile of the adsorbent CaNiAl-LDH.

VI. 3.5 Field Emission Scanning Emission Microscopy

The FE-SEM images of pristine CaNiAl-LDH at different scale sized (100 nm, 200 nm, 1 μm) are illustrated in **Fig VI.5**. The synthesized LDH showed a smooth structure with a circular and flower petals like shape with an average size below 300 nm. The uniform distribution of the LDH particle over the adsorbent surface can be ruled out from **Fig VI.5**. The images also reflect the formation of characteristic LDH platelets with many pores existing in them, which could be responsible for and contribute to the good adsorption performance of the material.[22,23]

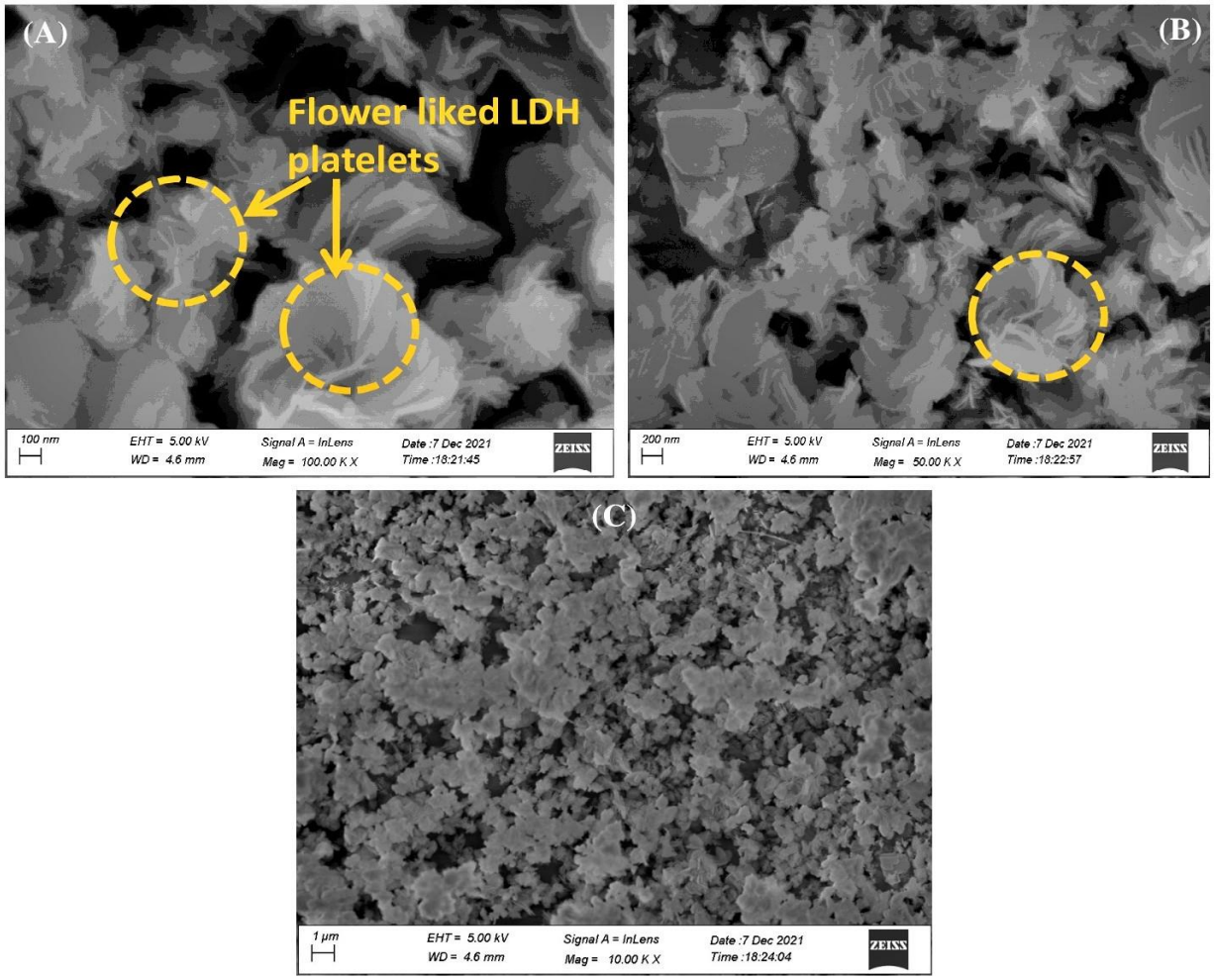

Fig VI.5: FE-SEM images of the adsorbent at different magnifications (100 nm, 200 nm and 1µm).

VI.4.1 Adsorption Isotherm

In isotherm studies, the three most widely used models, namely Langmuir,[24] Freundlich,[25] and Temkin,[26] were employed for investigating the sorption behaviour of CR dye on ternary CaNiAl-LDH. Based on the Langmuir model, it is assumed that adsorption of the solute molecules over the homogeneous surface takes place through the formation of monolayers, while the Freundlich model explains the adsorption process where the development of multiple layers occurs on the heterogeneous surface. The non-linear expressions for Langmuir, Freundlich, and Temkin models are given as follows:

$$q_e = \frac{q_{max}\, C_e K_l}{1+K_l C_e} \quad (6.4)$$

$$q_e = K_f C_e^{\,1/n} \quad (6.5)$$

$$q_e = B_T \ln (K_T C_e) \quad (6.6)$$

where, C_e(mg/g) is the equilibrium concentration of dye solution, q_{max} is the maximum monolayer adsorption capacity, and K_l and K_f are the Langmuir constant and Freundlich constant, respectively. The index n indicates the intensity of adsorption; B_T and K_T are the Temkin constants, which signifies the heat of adsorption and the equilibrium binding constant.

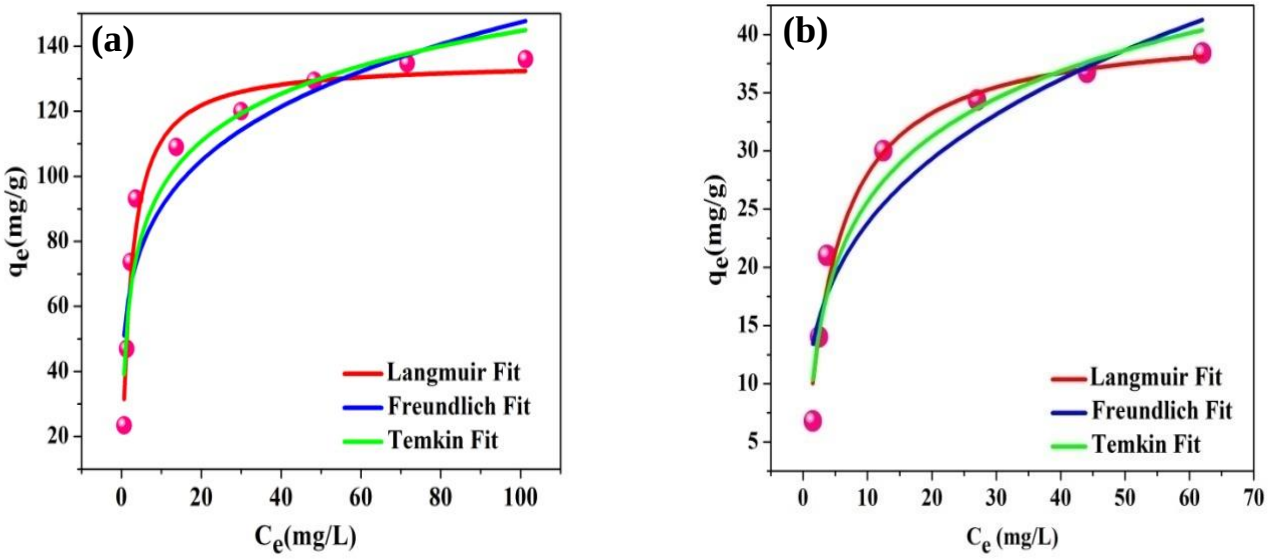

Fig VI.6: Non-linear adsorption isotherm curves based on Langmuir, Freundlich and Temkin model for adsorption of (a) Congo red dye (b) Methyl orange dye.

Fig VI.6 demonstrates the non-linear fitting of adsorption isotherm data for the sorption of CR and MO onto CaNiAl-LDH. The isotherm parameters are listed in **Table VI.1**. It is clearly seen that the co-efficient of determination for Langmuir (R^2 = 0.972) was found to be higher than other isotherm models such as Freundlich (R^2 = 0.850) and Temkin (R^2 = 0.926) for congo red adsorption. The maximum monolayer adsorption capacity of 135.21 and 40.93 mg/g was evaluated for CR and MO dye, respectively. The adsorption of both dyes onto CaNiAl-LDH was more suitable and can be best described according to Langmuir model, which further manifested that adsorption occurred more likely through single layer formation.

Table VI.1: Adsorption isotherm parameters determined by Langmuir, Freundlich and Temkin models.

Isotherm Model	Isotherm constant	Congo red	Methyl orange
Langmuir	q_{max} (mg/g)	135.21 ± 3.63	40.93 ± 1.58
	K_l(L/mg)	0.4543±0.05	0.2165 ± 0.03
	R^2	0.972	0.974
Freundlich	K_f(mg/g)(L/mg)$^{1/n}$	55.59 ± 7.51	11.88 ± 2.26
	n	4.72 ± 0.82	3.31 ± 0.61
	R^2	0.850	0.87
Temkin	B_T	21.07 ± 2.08	8.078 ± 0.74
	K_T	9.581 ± 4.65	2.392 ± 0.76
	R^2	0.926	0.951

Experimental conditions: C_0 = 30-270 mg/L (CR), 10-110 mg/L (MO), volume = 20 mL, dosages = 0.025 g, temperature = 28 °C, time = 6 h, q_{max} = Maximum monolayer adsorption capacity, K_l = Langmuir constant, K_f, n = Freundlich constant, B_T, K_T = Temkin constant

The feasibility of the adsorption process was predicted by a separation factor (R_L) which can be estimated by the equation

$$R_L = \frac{1}{1+K_l C_0} \qquad (6.7)$$

The graph of R_L vs $C_0$was displayed in **Fig VI.7(a,b)**. The evaluated value of R_L lies in the range of 0-1 for initial CR dye concentration (30-270 mg/L) and MO (10-110 mg/L). Thus, the obtained results indicate that adsorption was favourable.[27]

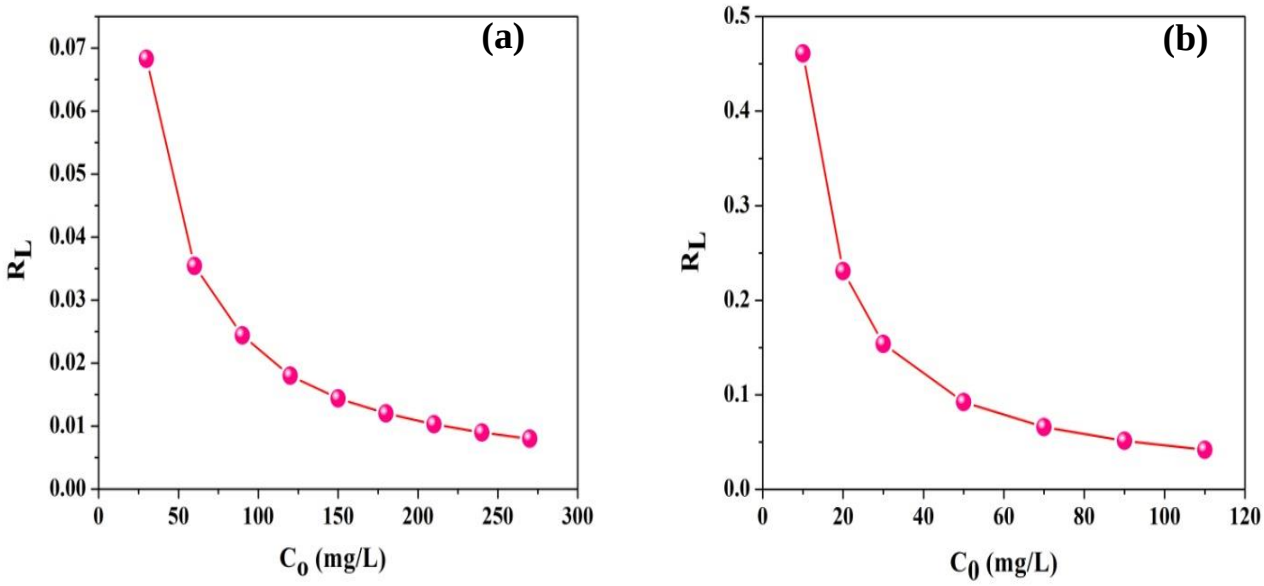

Fig VI.7: R_L vs C_0 plot for congo red and methyl orange dye uptake over CaNiAl-LDH.

VI.4.2 Adsorption Kinetics

To understand the adsorption rate of dyes and the dynamics associated with the process, kinetic studies were executed. The kinetics model applied for investigating dye adsorption on CaNiAl-LDH were pseudo-first-order,[28] pseudo-second-order,[29] and intraparticle diffusion.[30] The linearized equations for the respective models are given by:

$$\log (q_e - q_t) = \log q_e \ - \frac{K_1\, t}{2.303} \qquad (6.8)$$

$$\frac{t}{q_t} = \frac{1}{K_2 q_e^2} + \frac{t}{q_e} \qquad (6.9)$$

$$q_t = K_i\, t^{0.5} + C \qquad (6.10)$$

where, q_e is the quantity of dye adsorbed at equilibrium (mgg^{-1}), q_t indicates the quantity of dye adsorbed at time t (mgg^{-1}), K_i represents the intraparticle diffusion constant, and C is the boundary layer thickness.

The kinetics parameters for CR and MO dye adsorption were summarized in **Table VI.2**. The best fit of the kinetic model was determined by comparing the coefficient of determination (R^2) value. It is obvious from **Table VI.2** that R^2 value (0.919) for pseudo-first-order was found to be lower than for pseudo-second-order (0.998) in CR adsorption, which indicates the suitability of experimental data based on pseudo-second-order model. The experimental q_e(exp)(mg/g) value was also closer to q_{e2}(mg/g) than q_{e1}(mg/g). Thus, the adsorption kinetics can be well explained with a pseudo-second-order model, thereby indicating the presence of chemisorptions.[31] Similarly, the kinetics of MO dye adsorption also follows pseudo-second-order, as evident from the obtained results. The linear fitting of kinetics data for the CR and MO dye system has been displayed in **Fig VI.8** and **Fig VI.9**, respectively.

Table VI.2: Kinetic parameters for the adsorption of CR and MO dye on to CaNiAl-LDH.

Kinetics model	Parameters	Congo red	Methyl orange
Pseudo-first-order	q_e(exp)	38.396	30.40
	q_{e1}(mg/g)	18.927	10.09
	K_1 x 10^{-2} (min^{-1})	1.1561	0.690
	Δq	0.1406	0.3857
	R^2	0.919	0.909
Pseudo-second-order	q_{e2}(mg/g)	41.152	29.94
	K_2 x 10^{-3} ($g.mg^{-1}min^{-1}$)	1.0724	0.327
	Δq	0.0199	0.0087
	R^2	0.998	0.994
Intraparticle diffusion	K_i ($mg/g.min^{-1}$)	1.620	0.780
	C (mg/g)	15.245	17.74
	R^2	0.774	0.784

Experimental conditions: Initial concentration (C_0) = 50 mg/L, dosages = 0.025 g, volume = 20 mL, time = 260 min

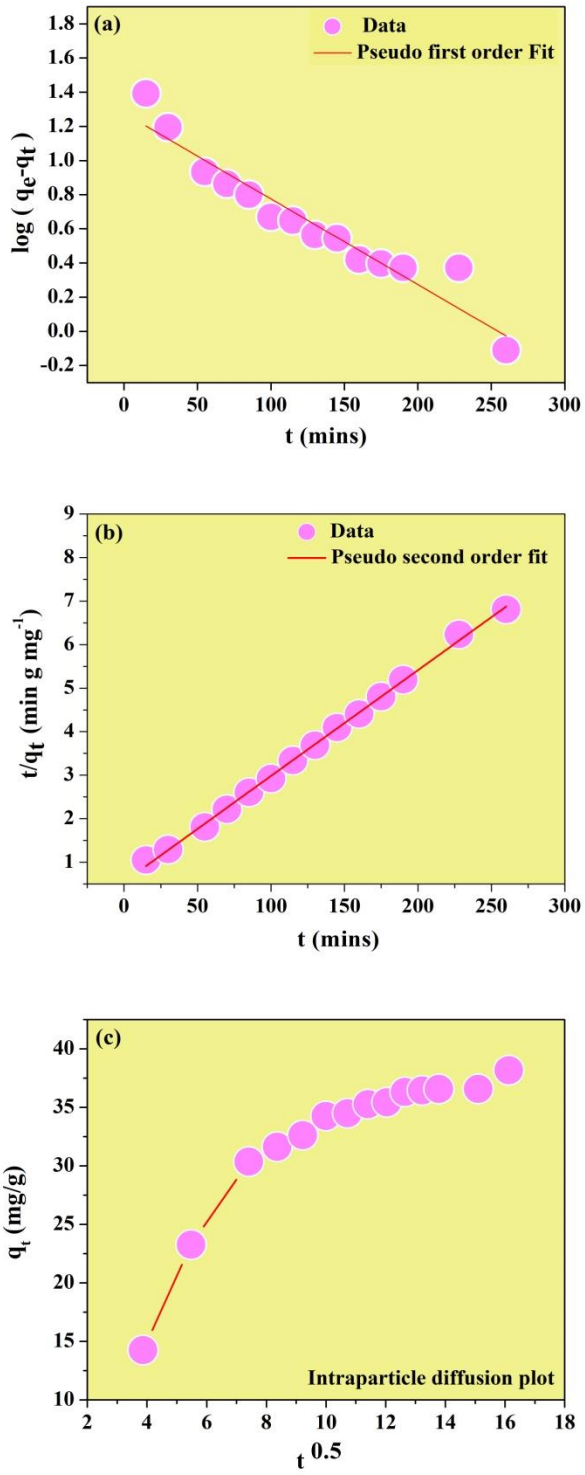

Fig VI.8: Kinetics plot of CR sorption (a) Pseudo-first-order (b) Pseudo-second-order (c) Intraparticle diffusion model.

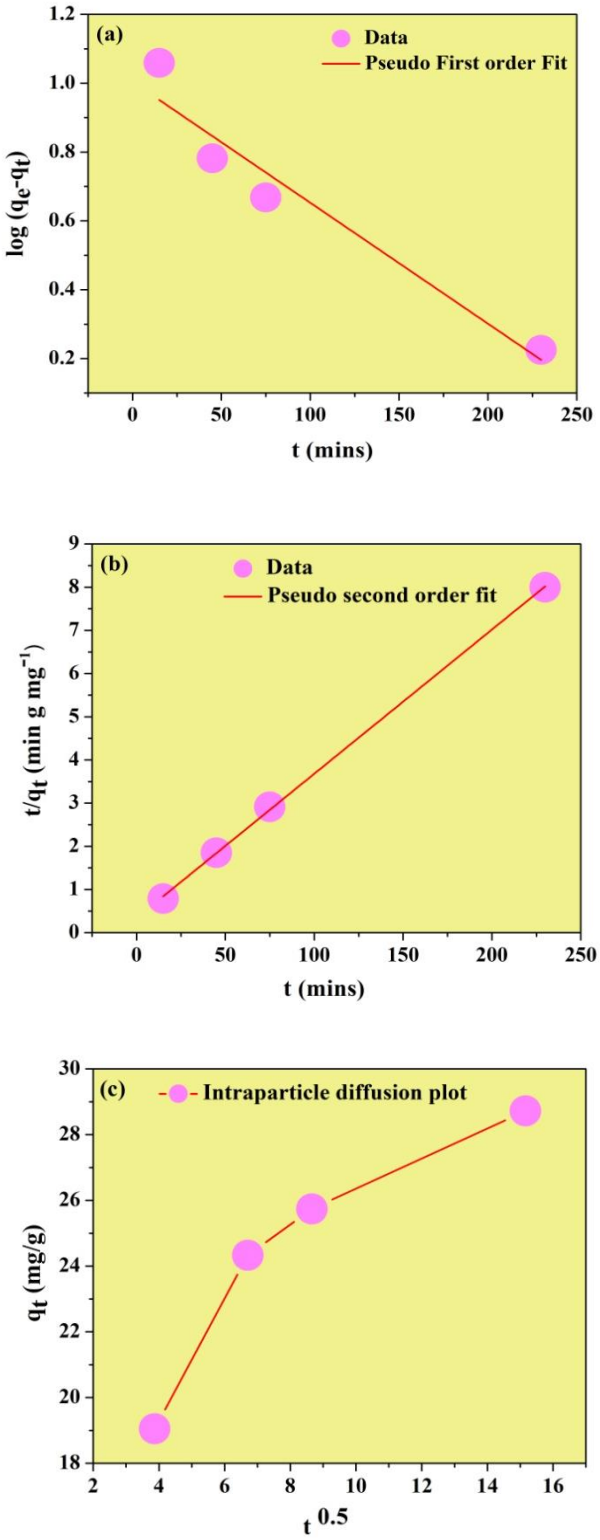

Fig VI.9: Kinetics plot of MO sorption (a) Pseudo-first-order (b) Pseudo-second-order (c) Intraparticle diffusion model**.**

Fig VI.8(c) shows the intraparticle diffusion plot ($q_t$vs $t^{0.5}$), which indicates the presence of multiple stages during the sorption of CR dye. The $q_t$value between ($t^{0.5}$ = 0.385-0.833) increased quickly, while in the middle region, bending of curves occurs due to diffusion into external pores. At the last stage, it tends to a constant straight line due to the achievement of equilibrium. Since the plot of $q_t$vs $t^{0.5}$ did not pass through the origin in both dye system, therefore the intraparticle diffusion is not the rate-limiting step.[32]

VI.4.3 Effect of Contact Time

The effect of contact time plays a key role in dye uptake. The removal efficiency of the adsorbate species as a function of contact time was investigated by fixing the experimental conditions with a 50 mg/L initial concentration, 0.025 g dosages, and a contact time of 260 mins, respectively. As shown in **Fig VI.10(a)**, it is apparent that the adsorption rate occurs rapidly in the first 70 minutes, when the adsorption capacity (q_t) reaches up to 31.62 mg/g. This can be explained due to the easily available active site at the initial stage of contact time, which is followed by the steric repulsion of incoming CR dye molecules on the sorption site, thereby leading to the equilibrium stage after 175 mins.[33] On the contrary, methyl orange sorption was rapid for the first 50 mins, where q_t value was 24.27 mg/g, and achieves equilibrium after 200 mins.

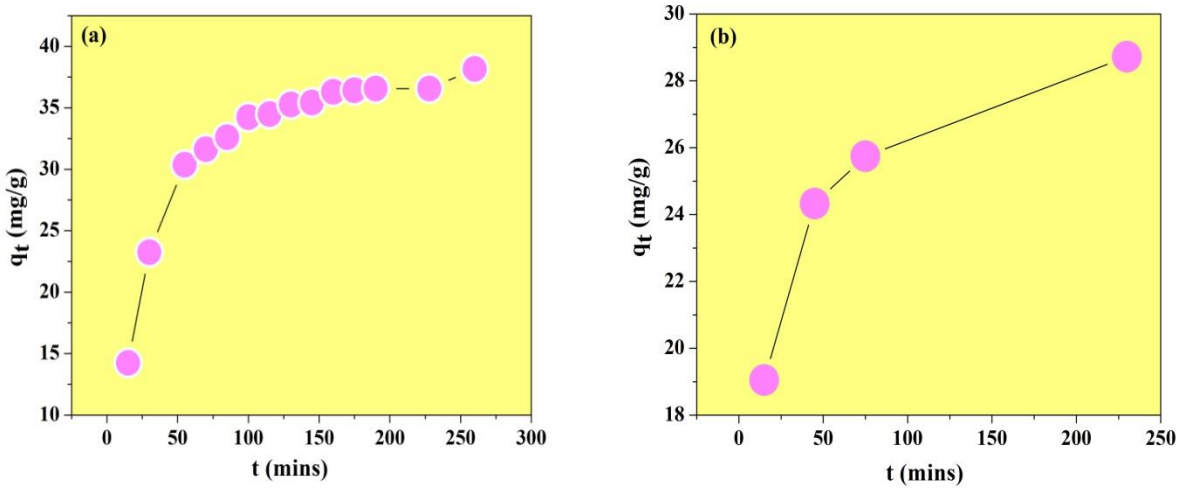

Fig VI.10: Effect of contact time for CR and MO adsorption onto CaNiAl-LDH.

VI.4.4 Effect of Adsorbent dosages

In order to maintain cost-effective system, estimation of the optimum dosages is very crucial. The effect of dosages was analysed by varying the amount of adsorbent from 0.005 g to 0.03 g for initial dye concentration of 50 mg/L. The quantity of dye adsorbed (q_e) decreases from 170.16 to 32.44 mg/g, and the removal percentage elevates from 85.08 to 97.34 %, as represented in **Fig VI.11**. After 0.02 g dosages, the removal efficiency does not increase significantly and remains constant. It is due to the fact that further increases in the applied adsorbent quantity may results in the accumulation of LDH particles, which will not promote the sorption of CR dye.[34] Nevertheless, in the case of MO-CaNiAl-LDH system, the removal % is 78 % at 0.025 g, and beyond these dosages there is no remarkable increment in removal %.

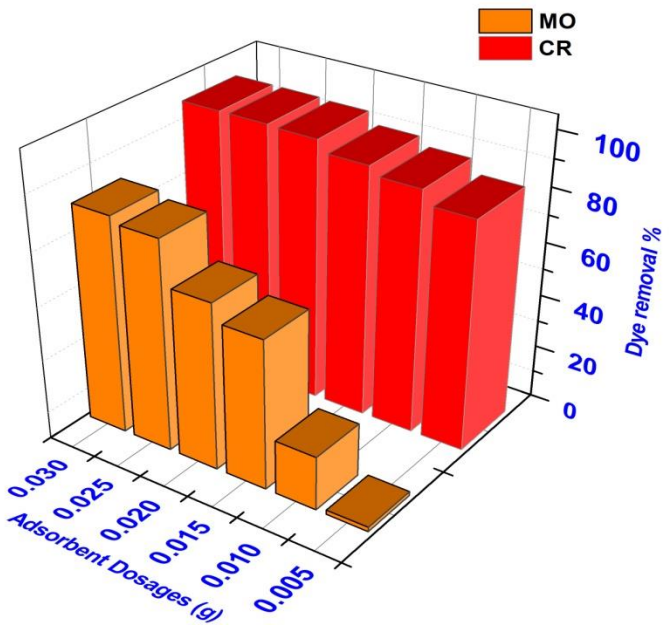

Fig VI.11: Effect of adsorbent dosages on CR and MO adsorption.

VI.4.5 Effect of pH

The solution pH plays a significant role in the adsorption process by altering the surface charge of the sorbents and the ionisation of the adsorbate ions. The interaction of the positively charged adsorbent surface with the negatively charged adsorbate ions is found to be highly sensitive to the pH of solution and provide further insight into the adsorbate-adsorbent system. In the present study, CR and MO dye was selected as adsorbates, and considering the effect of pH,

the removal % were analyzed under pH 4, 7, and 10 as shown in **Fig VI. 12(a, b)**. The maximum removal % at pH 4, 7, and 10 corresponding to the initial CR dye concentration (30 mg/L) were 97, 95.7, and 80%, respectively. Under acidic pH 4, the surface of CaNiAl-LDH bears additional +v e charge due to protonation (H_3O^+) from the solution. As a result, the electrostatic attraction between anionic CR ions and the positive charge LDH surfaces increases the sorption %. On the contrary, at a basic pH, due to the presence of competing negatively charged OH^- ions, the adsorption of incoming CR ions on the active site declines. Similarly, the removal % of MO dye can be described and was also very high at pH 4 compare to the basic pH. Thus, the pH of the solution during the studies showed a notable effect.[35]

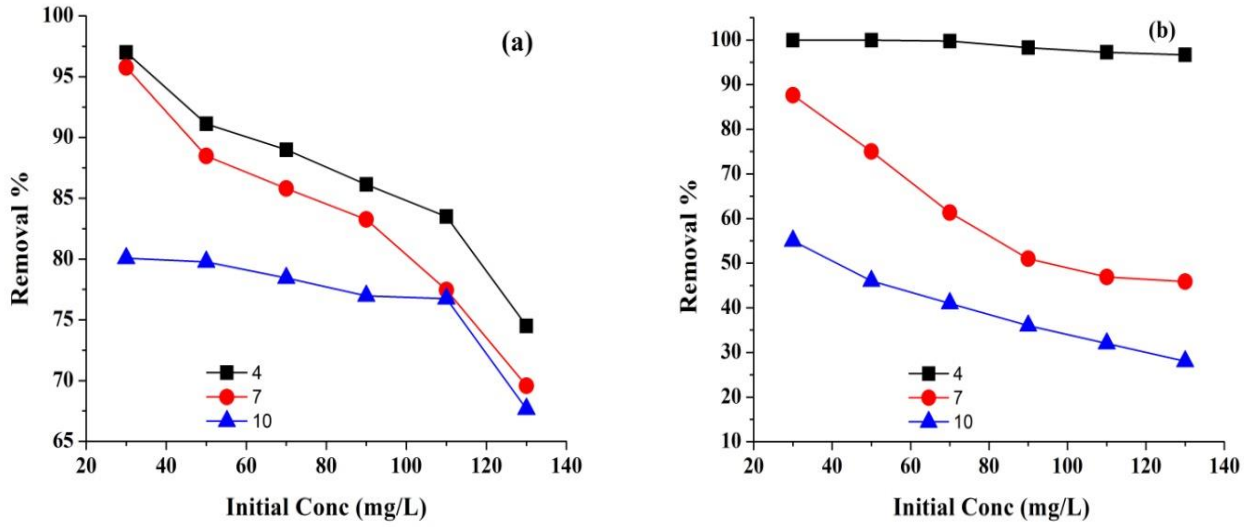

Fig VI.12: Effect of pH on the removal % of CR (a) and MO (b) dye.

VI.4.6 Thermodynamic Studies

The thermodynamic studies were carried out for the adsorptive removal of CR dye at various temperatures (40, 50, 60 ℃) using ternary CaNiAl-LDH adsorbents. For MO dye, the adsorption was not favourable with temperature and was not reported. The thermodynamic parameters such as Gibbs free energy (ΔG), enthalpy (ΔH), and entropy (ΔS) provide essential information regarding the feasibility of adsorption process. As a result, the estimation of these parameters was executed by using the following equations:[36]

$$\ln K_d = \frac{\Delta S}{R} - \frac{\Delta H}{RT} \quad (6.12)$$

$$\Delta G = -RT \ln K_d \quad (6.13)$$

where, K_d indicates the adsorption distribution coefficient and R denotes the universal gas constant. The values of enthalpy change (ΔH) and entropy change (ΔS) were measured from the slope and intercept of the graph ln K_d vs 1/T(K^{-1}), respectively.

The Vant-Hoff plot was displayed in **Fig VI.13**, and the obtained thermodynamic parameters are listed in **Table VI.3**. The negative value of ΔG was noted, which implies that CR adsorption onto CaNiAl-LDH was a spontaneous and feasible process. As the temperature increased from 313 K to 333 K, the ΔG value was found to decrease from -2.14 KJ/mol to -6.31 KJ/mol, thereby indicating a favourable adsorption process at the higher temperature. However, the endothermic nature of adsorption was manifested from the +ve value of ΔH, and the increase in randomness of the solid-liquid interfaces was confirmed from the +ve ΔS value. In general, for the chemisorption process, the magnitude of ΔH ranges between 80 and 200 KJ/mol, and the measured ΔH value (63.1 KJ/mol) in the current studies lies below the range. Thus, the process of CR adsorption on CaNiAl-LDH was predicted to occur through physisorption.[37]

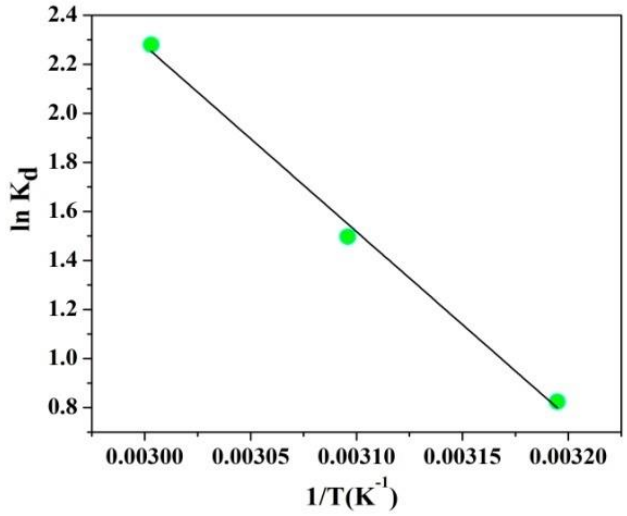

Fig VI.13: Vant-Hoff plot for estimating thermodynamic parameters in CR adsorption.

Table VI.3: Calculated thermodynamic parameters for the CaNiAl-LDH-CR system.

Adsorbent	+ΔH(KJ/mol)	+ΔS(J/mol)	-ΔG(KJ/mol)		
			313K	323K	333K
CaNiAl-LDH	63.038	208.032	2.14	4.02	6.31

Experimental Conditions and thermodynamic parameters: Initial Concentration(C_0) = 50 mg/L, dosages = 0.025 g, contact time = 4 hrs, temperature = 313K, 323 K, 333K, ΔG = Gibbs free energy, ΔH = Enthalpy, ΔS = Entropy

VI.4.7 Comparison with reported adsorbents:

In the previous report, various modified LDH listed in **Table VI.4** showed the removal of CR dye from an aqueous solution. However, in current studies, it is noteworthy that the employment of ternary CaNiAl-LDH manifests greater adsorption capacity (135.21 mg/g) as compared to several adsorbents such as Mg-Fe-Al-LDH, MgAl-LDH, MNPs@NiFe-LDH, and DS-Zn-Y hydroxide.[38, 39-44] Therefore, the comparative result shows the feasibility of CaNiAl-LDH as an effective adsorbent in CR removal.[45]

Table VI.4: List of reported LDH based sorbents with their q_{max} value for CR removal.[37-44]

Adsorbents	q_{max} (mg/g)	References
MgAl-LDH	111.11	[37]
LDH-EDTA-AM	632.9	[38]
Mg-Fe-Al-LDH	11	[39]
ZnAl-LDH	571.43	[40]
Mg-Fe-CO_3-LDH	104.6	[41]
MNPs@NiFe-LDH	79.6	[42]
β-$Ni(OH)_2$/γ-Fe_2O_3/NiFe-LDH	98.6-142.4	[43]
DS-Zn-Y hydroxide	96.24	[44]
CaNiAl-LDH	135.21	This work

VI.4.8 Reusability

To determine the potentiality of the proposed adsorbents for industrial applications, the reusability test in the adsorption process was examined only for CR dye due to poor adsorption of MO dye. For good adsorbents, repeated use does not significantly decline their affinity for targeted contaminants. In the current studies, the reusability test was investigated up to the fifth cycle. **Fig VI.14** revealed that the removal efficiency decreases from 95.73% to 75.99% as the recycle proceeds from the first to the last cycle. However, it is note worthy that the high sorption % of adsorbate molecules up to 75.99%, was maintained even after the fifth cycle, which shows its excellent performance for CR sorption. The slight decrease in removal percentage after successive uses might be attributed to the loss of active sites during regeneration.

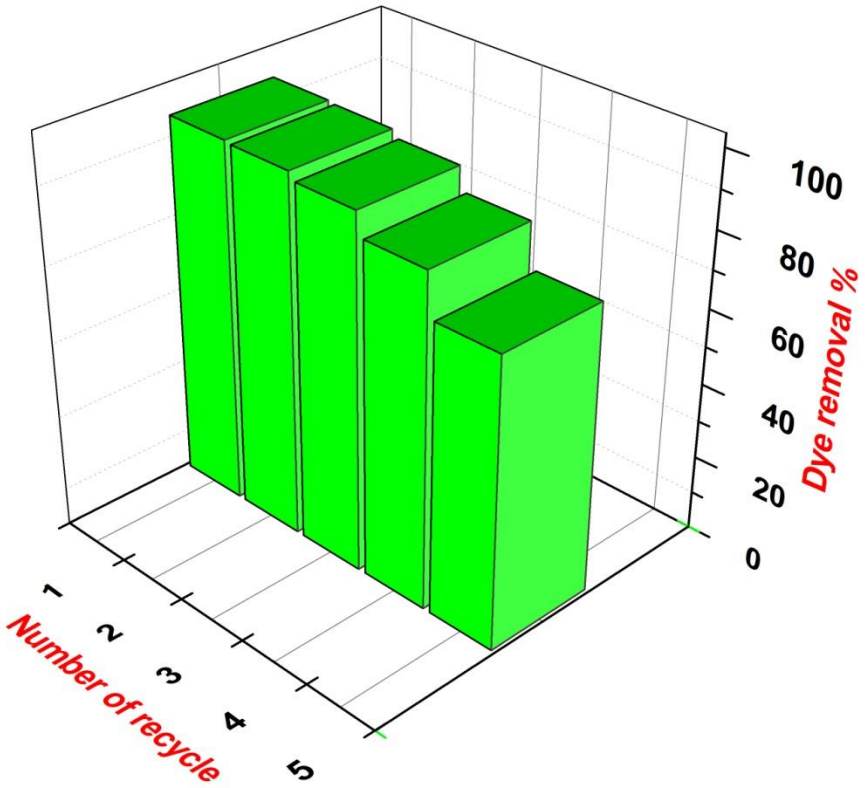

Fig VI.14: Reusability efficiency of ternary CaNiAl-LDH in the removal of Congo red dye from an aqueous solution.

VI.5 Conclusion

In summary, a ternary CaNiAl-LDH was synthesized by the urea hydrolysis method and applied to the treatment of aqueous solutions by selecting CR and MO as targeted pollutants. The unique physico-chemical properties of the proposed adsorbent CaNiAl-LDH, such as porosity, high surface area, and flower-shaped LDH particles, have contributed to the enhance sorption of CR dye compared to MO. Moreover, the isotherm and kinetics data fitted well according to the Langmuir and pseudo-second order kinetic models for both dyes. The adsorption capacity of CR dye over CaNiAl-LDH was found to be higher compared to MO dye. However, the removal of MO dye was also thermodynamically unfavourable, whereas the removal % increases for CR dye with increasing temperature. In addition, the main factor responsible for the adsorption of CR and MO dye may be due to the electrostatic attraction between the positively charged brucite sheets of LDH and negatively charged CR dyes. Besides, the existences of weak forces such as H-bonding and Vander Waals force can also be predicted in the adsorbate-adsorbent system. Thus, the present study sheds light on exploring ternary LDH and suggests that CaNiAl-LDH can be use as an alternative adsorbent for the treatment of dye-contaminated waste water.

VI.6 References

1. G.M. Ziarani, R. Moradi, N. Lashgari, H.G. Kruger, *Metal-Free Synthetic Organic Dyes*, Elsevier, **2018**, ch. 4, pp. 47-93.
2. D. Iark, A.J. dos Reis Buzzo, J.A.A. Garcia, V.G. Correa, C.V. Helm, R.C.G. Correa, R.A. Peralta, R.F.P.M. Moreira, A. Bracht, R.M. Peralta, *Bioresource Technology*., 289, **2019**, 121655.
3. S.S. Yang, J.H. Kang, T.R. Xie, D.F. Xing, N.Q. Ren, S.H. Ho, W.M. Wu, *Journal of Cleaner Production.*, 227, **2019**, 33.
4. C.Y. Teh, P.M. Budiman, K.P.Y. Shak, T.Y. Wu, *Ind. Eng. Chem. Res.*, 55, **2016**, 4363.
5. A.B. Fradj, A. Boubakri, A. Hafiane and S.B. Hamouda, *Results in Chemistry.*, 2, **2020**, 100017.
6. S. Venkatesh, K. Venkatesh, A.R. Quaff, *Journal of applied research and technology.*, 15, **2017**, 340.
7. S.Y. Lee, D. Kang, S. Jeong, H.T. Do, J.H. Kim, *ACS Omega.*, 5, **2020**, 4233.
8. A.K. Badawi, M.A. Elkodous, G.A.M. Ali, *RSC Adv.*, 11, **2021**, 36528.
9. Y. Tanimoto, S.I. Noro, *RSC Adv.*, 11, **2021**, 23707.
10. R.A.E.G. Mansour, M.G. Simeda, A.A. Zaatout, *RSC Adv.*, 11, **2021**, 7851.
11. W. Huang, S. Wang, D. Li, *Sustainable Polymer Composites and Nanocomposites*, e.d Inamuddin, S. Thomas, R.K. Mishra, A.M. Asiri, Springer Cham, **2019**, pp. 519-556.
12. S. Radoor, J. Karayil, A. Jayakumar, D. Nandi, J. Parameswaranpillai, J. Lee, J.M. Shivanna, R. Nithya, S. Siengchin, *J. Polym. Environ.*, 30, **2022**, 3279.
13. P. Huang, J. Liu, F. Wei, Y. Zhu, X. Wang, C. Cao, W. Song, *Mater. Chem. Front.*, 1, **2017**, 1550.
14. M. Khorshidi, S. Asadpour, N. Sarmast and M. Dinari, *J. Mol. Liq.*, 348, **2022**, 118399.
15. M. Daud, A. Hai, F. Banat, M.B. Wazir, M. Habib, G. Bharath, M.A.A. Harthi, *J. Mol. Liq.*, 288, **2019**, 110989.
16. L.J. Foruzin, Z. Rezvani, B. Habibi, *Appl. Clay Sci.*, 188, **2020**, 105511.
17. G. Rathee, N. Singh, R. Chandra, *ACS Omega*., 5, **2020**, 2368.
18. T.R.R. Timoteo, C.G. de Melo, L.J. de Alencar Danda, L.C.P.B.B. Silva, D.A.F. Fontes, P.C.D. Silva, C.S.B. Aguilera, L. da Paixao Siqueira, L.A. Rolim, P.J.R. Neto, *Appl. Clay Sci.*, 180, **2019**, 105197
19. D. Bharali, R.C. Deka, *J. Environ. Chem. Eng*., 5, **2017**, 2056.
20. S.S. R, A. Jana and S. De, *J. Hazard. Mater.*, 373, **2019**, 791.
21. M.A. Iqbal, L. Sun and M. Fedel, *SN Appl. Sci.*, 1, **2010**, 1415.
22. Z. Wang, L. Zhang, P. Fang, L. Wang, W. Wang, *ACS Omega*., 5, **2020**, 21805.
23. H. Lv, H. Rao, Z. Liu, Z. Zhou, Y. Zhao, H. Wei, Z. Chen, *J Energy Storage*., 52, **2022**, 104940.
24. I. Langmuir, *J. Am. Chem. Soc.*, 40, **1918**, 1361.
25. H. Freundlich, *J. Phys. Chem*., 57, **1906**, 385.
26. M.I. Temkin, V. Pyzhev, *Acta Physiochimica URSS.*, 12, **1940**, 327.
27. M.K. Raman, G. Muthuraman, *Asian J. Chem*., 31, **2019**, 1255.
28. S. Lagergren, *Kungl. Svenska Vetenskapsakad. Handl*., 24, **1898**, 1.
29. Y.S. Ho, G. Mckay, *Chem. Eng. J*., 70, **1998**, 115.

30. W.J. Weber, J.C. Morris, *J. Sanit. Eng. Div*., 89, **1963**, 31.
31. J.M. Jabar, Y.A. Odusote, K.A. Alabi, I.B. Ahmed, *Appl.Water Sci*., 10, **2020**, 136.
32. F.C. Wu, R.L. Tseng, R.S. Juang, *Chem. Eng. J*., 153, **2009**, 1.
33. H.T.N. Thi, D.C. Nguyen, T.T. Nguyen, V.T. Tran, H.V. Nguyen, L.G. Bach, D.V.N. Vo, D.H. Nguyen, D.V. Thuan, S.T. Do, T.D. Nguyen, *Key Engineering Materials*., 814, **2019**, 463.
34. D. Maiti, S. Mukhopadhyay, P.S. Devi, *ACS Sustainable Chem. Eng*., 5, **2017**, 11255.
35. A. Li, H. Deng, C. Ye, Y. Jiang, *ACS Omega*., 5, **2020**, 15152
36. B. Priyadarshini, T. Patra, T.R. Sahoo, *J. Magnes. Alloy*., 9, **2021**, 478.
37. R. Lafi, K. Charradi, M.A. Djebbi, A.B.H. Amara, A. Hafiane, *Adv. Powder Technol.*, 27, **2016**, 232.
38. J. Li, H. Yu, X. Zhang, R. Zhu, L. Yan, *Front. Environ. Sci. Eng.*, 14, **2020**, 52.
39. H.A. Tabti, B. Medjahed, M. Boudinar, A. Kadeche, N. Bouchikhi, A. Ramdani, S. Taleb, M. Adjdir, *Res. Chem.* Intermed., 48, **2022**, 2683.
40. S. Chilukoti, T. Thangavel, *Inorg. Chem. Commun.*, 100, **2019**, 107.
41. I.M. Ahmed, M.S. Gasser, *Appl. Surf. Sci*., 259, **2012**, 650.
42. T. Taher, R. Putra, N.R. Palapa, A. Lesbani, *Chem. Phys. Lett*., 777**, 2021**, 138712.
43. C. Suppaso, N. Pongkan, S. Intachai, M. Ogawa, N. Khaorapapong, *Appl. Surf. Sci.*, 213, **2021**, 106115.
44. P. Chakraborty, R. Nagarajan, *Appl. Surf. Sci*., 118, **2015**, 308.
45. D. Brahma, K.P. Nath, M. Patgiri, H. Saikia, *Asian J. Chem*., 35, 2022, 3215-3223.